Merging and Analysis of Elevation Time Series Over Greenland Ice Sheet From Satellite Radar Altimetry

Kirill S. Khvorostovsky

***Abstract*—Spatial–temporal variability and changes of Greenland ice sheet elevation from 1992 to 2008 are analyzed from merged ERS-1, ERS-2, and Envisat satellite radar altimeter data. A methodology for determining intersatellite biases was developed and applied in order to merge measurements from these different satellites and to create continuous and consistent time series. Intersatellite biases of elevation and backscatter coefficient have shown to be significantly affected by the bias between measurements in ascending and descending orbits. Adjustment of elevation time series for its dependence on backscatter coefficient and other waveform parameters performed in this paper substantially reduced the amplitude of elevation seasonal variations and locally corrected elevation change-rate estimates by up to several centimeters per year. It was found that the correction depends not only on the variations in the waveform parameters but also on the temporal variations of the correlation gradients, which represent the sensitivity of the elevation change to the change in the waveform parameters. An elevation change rate of $+2.8 \pm 0.2$ cm/year from 1992 to 2008 over 76% of the Greenland ice sheet area was found. Increases in surface elevation from 1995 observed over the high-elevation regions of Greenland were followed by an elevation decrease from 2006. For the whole period of 1992–2008, the elevation increase is 4.0 ± 0.2 cm/year over 87% of the area above 1500 m. In contrast, over 38% of the low-elevation areas below 1500 m, the rate of elevation change is -7.0 ± 1.0 cm/year, and the surface elevation decrease that started from 2000 has continued.**

***Index Terms*—Elevation change, Greenland ice sheet, satellite radar altimetry.**

I. Introduction

THE GREENLAND ice sheet is an important Earth-system component whose potential melting is critical for sea-level change and freshwater impact on ocean circulation. The mass balance of the Greenland ice sheet remains uncertain as there are discrepancies both between and within the following three main methods of mass balance estimation: 1) mass balance calculations (net input from snow and net losses from melting and ice discharge); 2) satellite gravimetric measurements such as the Gravity Recovery and Climate Experiment; and 3) surface elevation measurements over time using altimeters based on aircraft or satellite. Improvements in surface elevation measurements from satellite sensors can thus reduce this uncertainty (e.g., [1]). Satellite radar altimetry produces sufficient spatial coverage and density of the measurements needed to determine the changes of the Greenland ice sheet thickness [2]–[5]. Measurements of radar altimeters from a series of satellites (ERS-1, ERS-2, and Envisat) allow the investigation of the surface elevation changes of the Greenland ice sheet, excluding some ice sheet marginal areas, where the measurements are sparse due to rougher sloping surface.

This paper presents the following: 1) a methodology of merging of radar altimeter measurements from ERS-1, ERS-2, and Envisat satellites through estimation and applying intersatellite biases for creating continuous and consistent elevation time series and 2) spatial–temporal variability and trends derived from these new time series (1992–2008). Elevation time series are to be corrected for changes of the surface and subsurface scattering characteristics of the ice sheet by using their dependence on the received backscatter power and other parameters of the radar altimeter waveform shape [6]–[9]. Therefore, here, we also calculate biases between waveform parameters to create their time series along with the time series of surface elevation.

Spatially variable intersatellite bias between surface elevation measurements from ERS-1 and ERS-2 satellites was calculated by using different techniques and was applied for Greenland ice sheet elevation change estimation [3], [4]. Although elevation biases are correlated with the received backscatter power, surface slope, and surface elevation, it is "not possible to formulate the bias as a consistent function of these parameters over all of the ice sheet" [4]. Discontinuity of the characteristics of the received backscatter power—backscatter coefficient (σ^0) and automatic gain control (AGC)—obtained from radar altimeter measurements from ERS-1 and ERS-2 satellites over Greenland was noted in [10]. In addition, the determination of the intersatellite biases of elevation and waveform parameters becomes more complex when comparing the measurements on ascending and descending satellite tracks [11], [12]. In this case, it is necessary to account for ascending/descending (AD) bias that depends on the directions of the anisotropy of target and antenna polarization [13].

In order to correct elevation time series for changes in the ice sheet surface properties, the received backscatter power characteristics—σ^0 or AGC—were used in [4], [7], and [14]. Backscatter power as measured by satellite radar altimeters is affected by both surface and subsurface scattering characteristics that are themselves affected by surface roughness, snow density, and stratification [e.g., [15]]. Thus, adjustment of

Manuscript received August 31, 2010; revised March 4, 2011; accepted May 22, 2011. Date of publication August 1, 2011; date of current version December 23, 2011. This work was supported in part by the Research Council of Norway project "Greenland Ice Sheet Elevation (GreenISE): Integrated methodology using satellite, in situ and numerical modeling data" headed by Prof. O. M. Johannessen and in part by the Mohn–Sverdrup Center for Global Ocean Studies and Operational Oceanography at the Nansen Center through a donation from T. Mohn.

The author is with the Nansen Environmental and Remote Sensing Center, 5006 Bergen, Norway (e-mail: kirill.khvorostovsky@nersc.no).

Color versions of one or more of the figures in this paper are available online at http://ieeexplore.ieee.org.

Digital Object Identifier 10.1109/TGRS.2011.2160071

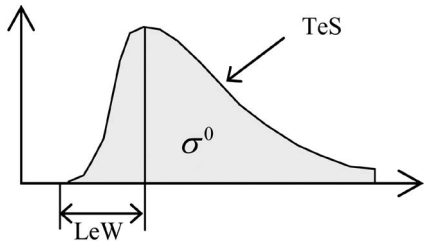

Fig. 1. Altimetric waveform shape parameters: backscatter coefficient (σ^0), LeW, and TeS. Adapted from [15].

elevation time series for its correlation with σ^0 corrects most of the spurious elevation changes introduced by variations of the snow properties. At the same time, Lacroix *et al.* [9] showed that the impact of some variations of the surface density and roughness on the altimeter signal may be corrected only by accounting for changes of the waveform shape parameters—leading edge width (LeW) and trailing edge slope (TeS) [15], [16] (see Fig. 1)—in addition to changes of σ^0. In particular, they studied rapid events occurring in the Vostok area (East Antarctica), which created a "jump" in the backscattered waveform parameters and the measured elevation associated with the removal of surface hoar by strong winds from an anomalous direction. In [6], [9], and [15], it was shown that waveform parameters show coherent signals in space and time, and their temporal variations are associated with meteorological events. At the same time, these studies showed that different parts of the waveform are controlled by different surface and subsurface characteristics: LeW is mostly dependent on the roughness and upper (few tens of centimeters) layer, whereas TeS is mostly related to the ratio between volume and surface echoes. Here, changes of σ^0 and other waveform parameters, as well as their relationship with elevation time series, are analyzed, and the effect of the correction on elevation change estimation is assessed.

II. Biases of Elevation and Waveform Parameters

A commonly used method for ice sheet elevation change studies is a crossover analysis using differences in elevation over the location where two orbit passes—ascending and descending—cross each other. Determination of intersatellite biases between measurements of any two satellites allows using a much larger amount of crossover points than using only crossover differences between measurements from the same satellite. Here, intersatellite biases of elevation, σ^0 and two parameters of the waveform shape—LeW and TeS—were estimated in order to form continuous time series of these parameters using measurements from ERS-1, ERS-2, and Envisat satellites. ERS-1 and ERS-2 ice-mode measurements and Envisat fine-mode measurements, which cover most of the Greenland ice sheet area [17], were used to create time series over grid cells 1° longitude $\times$ 0.5° latitude. ESA DORIS orbits for the Envisat satellite were used, while the other corrections applied for range measurements are the same as in [3].

Because the biases between altimeter measurements are spatially variable, it is more reasonable to estimate them with the same spatial resolution as that used in forming time series of elevation and waveform parameters, i.e., for the individual grid cells. ERS-1/ERS-2 and ERS-2/Envisat intersatellite biases can be determined by averaging crossover differences with small time intervals between measurements from different satellites. These crossovers are available during the periods of simultaneous operation of ERS-1 and ERS-2 altimeters, and ERS-2 and Envisat altimeters from May 1995 to May 1996 and from October 2002 to June 2003, respectively. However, the number of these crossovers is not sufficient in calculating the biases over large parts of southern and margin areas of the Greenland ice sheet. Therefore, Johannessen *et al.* [3] applied the technique using a linear regression fit of intersatellite elevation crossover differences (dH) to corresponding time differences (dt) for the calculation of ERS-1/ERS-2 elevation bias. Applying this regression method (RM), biases were estimated as an offset of the linear fit from the origin at the point where $dt = 0$. This method gave more reliable results by using a large number of crossovers formed using measurements from 1992 to 1996 and from 1995 to 1999 for the ERS-1 and ERS-2 altimeters, respectively. However, this technique accounts only for the linear trend of elevation change over the time period used for bias calculations, whereas the elevation trend may vary in time, thereby affecting bias estimation. This can be illustrated by the simplified case where elevation is generally constant in time during the period of measurements from the preceding satellite and during the first part of measurements from the subsequent satellite, and then, elevation starts to increase. When using crossover differences between measurements from different satellites related only to the period when the elevation was not changing, then the linear fit used for the calculation of the bias would be horizontal. However, involving measurements during the second part of the subsequent satellite would add larger crossover differences at the end part of the fit, and consequently, it would increase the slope of the fit and would lower the estimation of the bias. Although random variations of the elevation would average out this effect, deviations of the bias estimations may be important in some cases. Therefore, in order to account for temporal variations of elevation and waveform parameters, here we apply RM using a polynomial fit for crossovers with possibly small dt. The smallest dt that is sufficient in calculating a statistically significant value of the biases, as well as the order of the polynomial fit, was determined from an algorithm based on convergence of the calculated biases with increasing the order of the polynomial fit [18]. The criterion of convergence was applied because estimates of the bias using a higher order of polynomial fit should better account for temporal variation of crossover differences in situations where the amount of crossovers is sufficient and crossover differences are randomly distributed. The method of averaging crossover differences with $dt < 30$ days was applied for the calculation of the biases if the number of available crossovers was sufficient to obtain a result at a confidence level better than 95%; otherwise, RM was used.

In order to account for AD bias, we used two different sets of crossover differences to calculate two estimates for each of the intersatellite biases: $B_{\mathrm{ers2\_}a-\mathrm{ers1\_}d}$ and $B_{\mathrm{ers2\_}d-\mathrm{ers1\_}a}$ for each of the ERS-1/ERS-2 biases and $B_{\mathrm{env\_}a-\mathrm{ers2\_}d}$ and $B_{\mathrm{env\_}d-\mathrm{ers2\_}a}$ for the ERS-2/Envisat biases. One set of crossovers was obtained using differences between

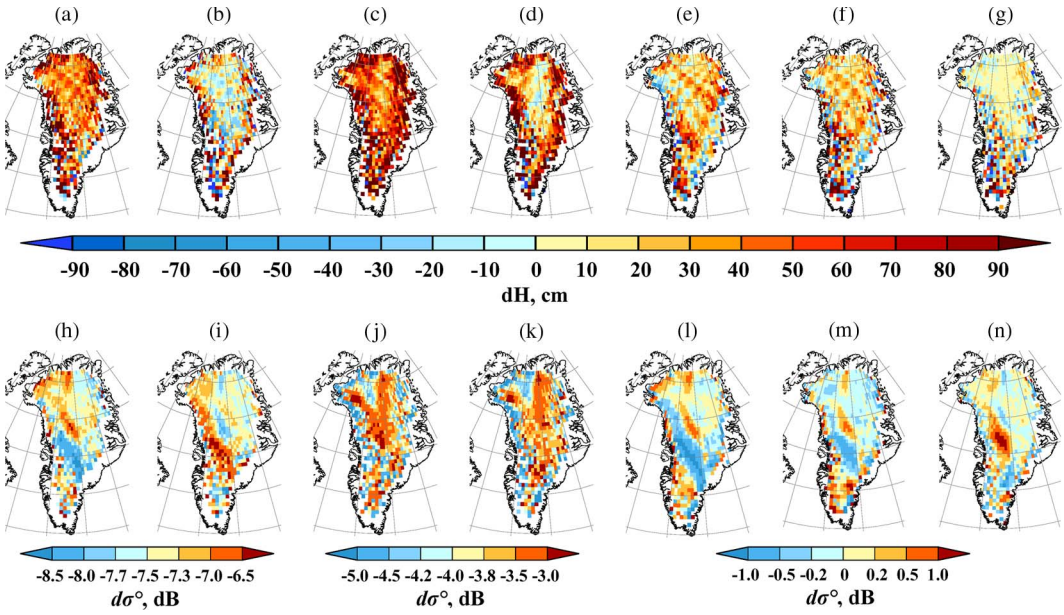

Fig. 2. Intersatellite and AD biases for (a)–(g) elevation and (h)–(n) σ^0. (a) and (h) $B_{\mathrm{ers2\_}d-\mathrm{ers1\_}a}$. (b) and (i) $B_{\mathrm{ers2\_}a-\mathrm{ers1\_}d}$. (c) and (j) $B_{\mathrm{env\_}d-\mathrm{ers2\_}a}$. (d) and (k) $B_{\mathrm{env\_}a-\mathrm{ers2\_}d}$. (e) and (l) $B_{\mathrm{ers1\_}d-\mathrm{ers1\_}a}$. (f) and (m) $B_{\mathrm{ers2\_}d-\mathrm{ers2\_}a}$. (g) and (n) $B_{\mathrm{env\_}d-\mathrm{env\_}a}$.

measurements in ascending orbits from one satellite and measurements in descending obits from another one, and vice versa for the second set. Then, when creating time series, one of the two estimates of each bias was applied to corresponding intersatellite crossovers. Thus, by involving a large amount of crossover points, we were able to take AD biases into account in addition to estimating the intersatellite biases with higher spatial resolution.

ERS-1/Envisat biases were estimated as a sum of other determined intersatellite biases and AD bias of ERS-2 measurements $B_{\mathrm{ere2\_}d-\mathrm{ers2\_}a}$

$$\begin{aligned} B_{\mathrm{env\_}a-\mathrm{ers1\_}d} &= B_{\mathrm{ere2\_}a-\mathrm{ers1\_}d} + B_{\mathrm{env\_}a-\mathrm{ers2\_}d} \\ &\quad + B_{\mathrm{ers2\_}d-\mathrm{ers2\_}a} \\ B_{\mathrm{env\_}d-\mathrm{ers1\_}a} &= B_{\mathrm{ere2\_}d-\mathrm{ers1\_}a} + B_{\mathrm{env\_}d-\mathrm{ers2\_}a} \\ &\quad - B_{\mathrm{ers2\_}d-\mathrm{ers2\_}a} \end{aligned}$$

where $B_{\mathrm{ere2\_}d-\mathrm{ers2\_}a}$ was calculated by the same methods used for intersatellite biases.

Before calculating the intersatellite elevation biases, spatially invariant offsets between measurements from different satellites were applied to the elevation crossover differences. When calculating ERS-1/ERS-2 biases, ERS-1 elevation measurements were lowered by 40.9 cm [19], whereas 73.68 cm was added to Envisat measurements (e.g., [20]) before estimating the ERS-2/Envisat elevation bias.

The range resolution in the ERS ice-mode measurements is about 4× lower than that in the Envisat fine-mode measurements. Therefore, to make the LeW and TeS values comparable, they were adjusted accordingly before estimating their ERS-2/Envisat biases. ERS-1/ERS-2 LeW and TeS biases were not observed. LeW was converted from waveform gates to meters, and TeS, determined as the exponential decay rate, was converted from per gates to per meters.

ERS-1/ERS-2, ERS-2/Envisat, and ERS-2 AD biases that were used in forming continuous time series exhibit significant spatial variability and features on different scales. These biases for elevation and σ^0 are shown in Fig. 2. The essential characteristic of intersatellite biases is a strong influence of AD biases. Therefore, when forming time series for elevation and waveform parameters, the specified biases should be applied to the corresponding intersatellite crossovers.

The main spatial feature of elevation intersatellite bias distributions is the largest and smallest values observed over margins and central areas, respectively [see Fig. 2(a)–(d)]. Biases vary from -1.8 to 3.4 m over Greenland, with standard deviations of 0.5 to 0.6 m. The effect of the AD biases results in significantly higher values of $B_{\mathrm{ers2\_}d-\mathrm{ers1\_}a}$ than $B_{\mathrm{ers2\_}a-\mathrm{ers1\_}d}$ and $B_{\mathrm{env\_}d-\mathrm{ers2\_}a}$ than $B_{\mathrm{env\_}a-\mathrm{ers2\_}d}$. These differences correspond to mostly positive ERS-1 ($B_{\mathrm{ers1\_}d-\mathrm{ers1\_}a}$), ERS-2 ($B_{\mathrm{ers2\_}d-\mathrm{ers2\_}a}$), and Envisat ($B_{\mathrm{env\_}d-\mathrm{env\_}a}$) AD biases calculated by subtracting measurements on ascending passes from measurements on descending ones (see Fig. 2(e)–(g) and Table I). The positive values of the means of the intersatellite elevation biases indicate that elevations measured from ERS-2 and Envisat satellites are, in average, higher than those measured by ERS-1 and ERS-2 altimeters, respectively (Table I).

Distributions of intersatellite σ^0 biases also have pronounced large-scale features [see Fig. 2(h)–(k)]. Although the means of the σ^0 biases $B_{\mathrm{ers2\_}d-\mathrm{ers1\_}a}$ and $B_{\mathrm{ers2\_}a-\mathrm{ers1\_}d}$ are similar (Table II), their distributions are opposite and mostly resulting from similar distributions of ERS-1 and ERS-2 AD biases [see Fig. 2(l) and (m)]. For ERS-2/Envisat σ^0 biases, their means and distributions are similar and correspond to the distributions of the ERS-2 and Envisat AD biases, which are of opposite sign [see Fig. 2(m) and (n)]. All intersatellite σ^0 biases are negative everywhere, ranging from -9.8 to -1 dB, with standard deviations of 0.5 to 0.9 dB.

ERS-2/Envisat LeW biases are, on average, -0.96 and -1.01 m for $B_{\mathrm{env\_}d-\mathrm{ers2\_}a}$ and $B_{\mathrm{env\_}a-\mathrm{ers2\_}d}$, respectively. They vary over Greenland between -3.8 and 0.2 m, with standard deviations of 0.46 and 0.48 m. ERS-2/Envisat TeS biases

TABLE I
AVERAGE INTERSATELLITE AND AD ELEVATION BIASES

Dataset	Elevation bias, cm	Cells	Area, 10^3 km^2	*dt* range[a], days	RM area[b], %
$B_{ers2\_d-ers1\_a}$	48.9 ± 1.9	836	1318.5	174 ± 11	32
$B_{ers2\_a-ers1\_d}$	15.7 ± 2.0	824	1294.6	246 ± 13	50
$B_{env\_d-ers2\_a}$	70.5 ± 1.9	866	1378.8	187 ± 12	32
$B_{env\_a-ers2\_d}$	51.9 ± 2.1	875	1392.5	174 ± 11	34
$B_{ers1\_d-ers1\_a}$	19.4 ± 1.4	923	1485.5	107 ± 5	33
$B_{ers2\_d-ers2\_a}$	19.9 ± 1.6	933	1507.6	85 ± 7	18
$B_{env\_d-env\_a}$	6.3 ± 1.2	923	1489.1	74 ± 5	20

[a]*dt* range is the average range of crossover time differences used for bias calculation.
[b]RM area – area, where bias was estimated using a regression method, in percents of the whole area, where the bias was obtained.

TABLE II
AVERAGE INTERSATELLITE AND AD BACKSCATTER COEFFICIENT(σ^0) BIASES

Dataset	σ° bias, dB	Cells	Area, 10^3 km^2	*dt* range[a], days	RM area[b], %
$B_{ers2\_d-ers1\_a}$	-7.49 ± 0.02	850	1341.1	96 ± 8	20
$B_{ers2\_a-ers1\_d}$	-7.31 ± 0.02	852	1344.7	85 ± 7	19
$B_{env\_d-ers2\_a}$	-3.89 ± 0.03	867	1385.8	127 ± 9	25
$B_{env\_a-ers2\_d}$	-3.91 ± 0.03	868	1384.3	107 ± 8	17
$B_{ers1\_d-ers1\_a}$	-0.07 ± 0.02	944	1526.8	99 ± 6	35
$B_{ers2\_d-ers2\_a}$	-0.01 ± 0.02	925	1495.0	60 ± 17	34
$B_{env\_d-env\_a}$	0.04 ± 0.02	926	1488.4	120 ± 7	35

[a] and [b] are the same as in Table I

range from -0.14 to 0.02 m^{-1}, with standard deviations of 0.02 m^{-1} and means of -0.01 m^{-1}. As well as for σ^0, the spatial distributions of the biases $B_{\mathrm{env\_}d-\mathrm{ers2\_}a}$ and $B_{\mathrm{env\_}a-\mathrm{ers2\_}d}$ are similar for LeW and TeS.

The percentage of the area where RM was applied is presented for elevation and σ^0 biases in Tables I and II. For different biases, it varies from 17% to 50% of the area where bias estimates are available. The percentage is largest for elevation biases due to the higher spatial variability of surface elevation within the individual cells, resulting also in a larger range of dt used for the calculation of the biases. Thus, both methods—the method of averaging crossover differences and RM—largely contribute to the determination of the biases.

Over ice sheet margins, where the quantity of the data is limited, only a few biases could be found for some cells. In this case, biases were estimated, if possible, using all available intersatellite crossovers, i.e., without accounting for AD bias. For elevation and σ^0 intersatellite biases, which are most affected by the AD biases, combined estimates were calculated, respectively, over 6% and 4% of the area, where all biases were found and time series of all parameters were formed. Thus, the time series obtained by merging altimeter measurements from ERS-1, ERS-2, and Envisat satellites were created using intersatellite biases over 840 cells covering an area of 1328.1×10^3 km^2.

In order to assess the accuracy of the bias estimates obtained by RM, they were compared with those calculated by the method of averaging crossovers with $dt < 30$ days, where they are available. Tables III and IV show the average differences and correlations for several estimates calculated on the basis of RM: using polynomial and linear fits, smallest possible dt range, and dt limited by seven years. The estimates that use the smallest possible dt range have a remarkably better correspondence to estimates based on the method of averaging than those obtained using large dt range: the correlations are higher, and the differences are less and more randomly distributed over

TABLE III
COMPARISON OF ELEVATION BIAS ESTIMATES CALCULATED BY RM METHODS AND METHOD OF AVERAGING CROSSOVER DIFFERENCES

Dataset	Cells	Area	Difference			Correlation coefficient				
			RM polyn small dt	RM linear small dt	RM linear large dt	RM polyn small dt	RM linear small dt	RM large dt		
								1[a]	2[a]	3[a]
$B_{ers2\_d-ers1\_a}$	621	903.7	-2.6±0.8	-4.3±0.7	-7.1±0.9	0.86	0.89	0.80	0.87	0.86
$B_{ers2\_a-ers1\_d}$	446	650.7	-5.0±0.8	-5.5±0.8	-7.1±1.1	0.91	0.94	0.85	0.91	0.92
$B_{env\_d-ers2\_a}$	636	934.9	-4.3±0.7	-3.6±0.7	-8.9±0.8	0.89	0.90	0.86	0.88	0.88
$B_{env\_a-ers2\_d}$	612	914.6	-5.8±0.8	-4.5±0.7	-11.3±0.9	0.91	0.93	0.88	0.91	0.92
$B_{ers1\_d-ers1\_a}$	659	1001.6	-0.1±0.6	-0.8±0.6	-2.7±1.0	0.92	0.93	0.79	0.88	0.88
$B_{ers2\_d-ers2\_a}$	781	1232.7	-0.1±0.5	-0.4±0.5	-0.03±0.5	0.94	0.95	0.94	0.94	0.94
$B_{env\_d-env\_a}$	752	1189.5	0.6±0.5	0.3±0.4	0.9±0.5	0.93	0.95	0.94	0.94	0.94

[a]Degrees of the polynomial fit applied for bias calculation when using RM and large *dt* range of crossover time differences

TABLE IV
COMPARISON OF BACKSCATTER COEFFICIENT(σ^0) BIAS ESTIMATES CALCULATED BY RM METHODS AND METHOD OF AVERAGING CROSSOVER DIFFERENCES

Dataset	Cells	Area	Difference			Correlation coefficient				
			RM polyn small dt	RM linear small dt	RM linear large dt	RM polyn small dt	RM linear small dt	RM large dt		
								1[a]	2[a]	3[a]
$B_{ers2\_d-ers1\_a}$	715	1073.4	-0.01±0.01	0.00±0.01	-0.16±0.02	0.90	0.88	0.60	0.60	0.60
$B_{ers2\_a-ers1\_d}$	725	1094.2	-0.02±0.01	-0.01±0.01	-0.13±0.02	0.78	0.82	0.40	0.64	0.70
$B_{env\_d-ers2\_a}$	696	1044.3	-0.04±0.01	-0.03±0.01	-0.19±0.03	0.89	0.90	0.56	0.76	0.81
$B_{env\_a-ers2\_d}$	756	1153.3	-0.05±0.01	-0.05±0.01	-0.18±0.03	0.91	0.92	0.54	0.79	0.85
$B_{ers1\_d-ers1\_a}$	646	985.2	0.00±0.01	-0.01±0.01	0.03±0.01	0.97	0.97	0.92	0.92	0.91
$B_{ers2\_d-ers2\_a}$	717	1114.7	0.01±0.01	0.00±0.004	-0.02±0.01	0.95	0.95	0.91	0.94	0.94
$B_{env\_d-env\_a}$	559	846.2	0.00±0.004	0.00±0.004	0.00±0.01	0.96	0.95	0.93	0.94	0.94

[a] is the same as in Table III

most of the Greenland ice sheet. The effectiveness of using polynomial fit is revealed from the estimates obtained using large dt, i.e., important in cases of a small amount of crossover points. For estimates obtained using dt limited by seven years, a closer correspondence with increasing degree of polynomial fit (to the third degree) is indicated for most of the intersatellite biases. Thus, both—using smallest dt and polynomial fit—are important when applying RM for the calculation of the biases.

By applying intersatellite biases to corresponding ERS-1 × ERS-2, ERS-2 × Envisat, and ERS-1 × Envisat crossover differences, three-month-averaged time series of elevation and waveform parameters from April 1992 to December 2008 were created for individual cells. The approach used in generating the time series is based on the technique described in [21] and [18]. In order to obtain a time series with a one-month resolution, three-month-averaged time series were created with one-month steps, i.e., time intervals represented by adjacent points are overlapping and lagging by one month. The resulting time series consist of 196 points, starting from interval April to June (AMJ) 1992 and ending with the interval October to December (OND) 2008. The three-point gap of no data from FMA to AMJ 2006 is due to Envisat radar altimeter sensor anomaly from February 8 to June 22.

Linear trends of elevation dH/dt over individual cells were obtained by fitting linear and sinusoidal functions to elevation time series, following the method used in [4] and [22]. In most elevation time series (93% of the studied area), the

linear-sinusoidal fit very well represents data with a probability less than 5% of a larger than calculated F-statistic value occurring by chance, i.e., significance level $\alpha < 0.05$. Moreover, linear trends for all cells were calculated with a significance level higher than 0.01. An average elevation change rate (dH/dt) of 3.4 cm/year was found for the time series obtained by applying the determined elevation biases.

In [5] and [14], continuous elevation time series from radar altimeter measurements over the Antarctic and Greenland ice sheets were created by adjusting together (merging) the time series obtained separately from different satellites. This approach avoids the necessity to apply intersatellite biases but ignores a large amount of intersatellite crossovers. Elevation change rates (dH/dt) obtained by applying intersatellite biases and by adjusting time series from different satellites on the basis of average time series for overlapping periods were compared [18]. Differences between dH/dt results show a good agreement for the central northern regions of Greenland—ranging within ± 1 cm/year—with values increasing toward the southern and coastal areas where the amount of available altimeter measurements is decreased. The average difference between the results of 0.09 ± 0.07 cm/year over regions where both results are available indicates a small influence of the approach used in merging the data from different satellites on the overall result.

III. Correction of Elevation Time Series For Their Dependence on Waveform Parameters

A. Correction Using Constant Correlation Gradient

One of the important corrections of elevation-change time series and their seasonal and interannual variations is the adjustment for the correlation of elevation changes with changes of backscattered power (σ^0 or AGC) [4], [7], [8] and with changes of all waveform shape parameters (σ^0, LeW, and TeS) [9]. When using only σ^0, this correction was determined here for each point i of time series over individual grid cells by the conventional method as a product of σ^0 change in point i $(d\sigma_i^0)$ and the gradient representing the sensitivity of the elevation change to the change in backscattered power $(dH/d\sigma^0)$. Then, the corrected elevation change dH_{i_cor} for point i was found by subtraction of the correction as

$$dH_{i\_\mathrm{cor}} = dH_i - (dH/d\sigma^0) \cdot d\sigma_i^0.$$

High correlation coefficients between the elevation and σ^0 time series for the Antarctic ice sheet were reported in two studies. In [7], correlations larger than 0.7 were found for most locations, and in [8], the average correlation was 0.64 over all studied areas, exceeding 0.7 only for half of the cells. Davis and Ferguson [8] speculated that the main factor resulting in this distinction is the differences of the following: 1) between satellite altimeter instruments (ERS-1 measurements were used in [7], and ERS-2 measurements were used in [8]) and 2) between retracking algorithms. At the same time, the length of the time period used for correlation and gradient determination seems to be an important cause of the observed difference. Whereas a five-year period (1995–2000) of ERS-2 satellite observations was used in [8], Wingham *et al.* [7] used only 18 months of ERS-1 data (June 1993–December 1994) in estimating the $dH/d\sigma^0$ gradient. Due to the discrepancy in temporal variations of elevation and σ^0, correlations may become weaker with the increasing length of the time period considered. For example, if the time series of elevation and σ^0 diverge after some point, then the correlation becomes weaker even if temporal variations are in agreement before and after this point. This could explain the higher correlation coefficient obtained in [7], where a shorter time period was used in estimating the correlation and gradient. At the same time, a low correlation generally corresponds to a low gradient $dH/d\sigma^0$ and, therefore, results in an underestimation of the correction.

This problem is more important for the Greenland ice sheet, where the temporal variability of elevation and backscattered power is higher than that over Antarctica due to a larger variability in accumulation and summer melting over low-elevation areas. Over Greenland, the average correlation coefficient between time series of elevation and σ^0 was found here to be $\sim$0.25 for the whole time period from 1992 to 2008. The correlation exceeds 0.7 only for some cells in the high-elevation areas, whereas over most of the studied area of Greenland, it is lower than 0.3.

To overcome the problem associated with high temporal variability, correlation gradients were estimated from time series constructed using the differences between adjacent points of time series

$$\Delta dH_i = dH_i - dH_{i-1} \;\; \Delta d\sigma_i^0 = d\sigma_i^0 - d\sigma_{i-1}^0, \;\; i = 2, \ldots, N$$

where N is the number of time intervals for which dH_i and $d\sigma_i^0$ are available. Time series points ΔdH_i and $\Delta d\sigma_i^0$ represent only changes between two adjacent points i and $i-1$ of the initial time series. Then, disagreements between any corresponding points of dH_i and $d\sigma_i^0$ time series do not affect the general agreement of the whole time series. The better overall agreement between the new time series results in a higher average correlation coefficient of 0.39 ± 0.01 and correlations higher than 0.5 over almost half of the studied area [see Fig. 3(a)]. The average correlation gradient $\Delta dH/\Delta d\sigma^0$ of 11.2 ± 3.8 cm/dB obtained from the new time series is about 1.3 cm/dB higher than the gradient obtained from original time series, thereby resulting in a higher absolute value of the correction of the elevation change. The correlation coefficient and correlation gradients correspond to each other, indicating, in general, higher and lower values over the central and margin areas, respectively [see Fig. 3(a) and (b)]. The effect of the correction on the estimation of dH/dt—i.e., differences between dH/dt trends before and after adjustment—is shown in Fig. 3(d). On average, corrections are 0.35 and 0.22 cm/year, with standard deviations of 0.8 and 1.0 cm/year when using $dH/d\sigma^0$ and $\Delta dH/\Delta d\sigma^0$ gradients, respectively. The corrections are small, on average, because of the low average σ^0 change rates $(d\sigma^0/dt)$, which amount to 0.01 dB/year. At the same time, as $d\sigma^0/dt$ values vary between ± 30 dB/year [see Fig. 3(c)], the corrections can be large locally, ranging from -3.2 to 3.4 cm/year when using $\Delta dH/\Delta d\sigma^0$ gradient.

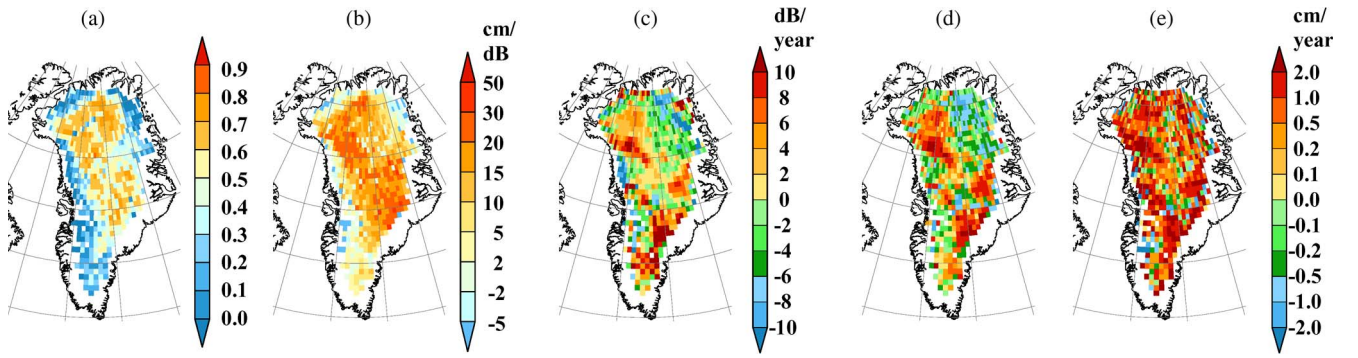

Fig. 3. Estimated as a constant within individual cells (a) correlation coefficients between ΔdH and $\Delta d\sigma^0$ time series, (b) corresponding correlation gradients, (c) $d\sigma^0/dt$ trends, and corrections of dH/dt trends for changes in (d) σ^0 and (e) all waveform shape parameters.

The correction of elevation change for its dependence on all waveform shape parameters, i.e., σ^0, LeW, and TeS, was found by applying multiple regression. Accounting for the combined impact of waveform parameter changes on the elevation time series resulted in a higher correction [see Fig. 3(e)]. This is primarily because LeW, which is negatively correlated with elevation time series, rapidly decreases, on average, by $\sim$0.3 m ($\sim$0.15 gate for the ERS ice-mode measurements) in summer 2002. This rapid fall is about twice as large as in the summers of the other years and is likely associated with increased melt anomaly that year. Spatially, the difference between corrections is mostly pronounced in the northeastern area of Greenland, where a negative change rate of σ^0 gives a negative correction [see Fig. 3(c) and (d)], whereas changes of LeW, when accounting for the combined effect of waveform parameters, give a positive correction [see Fig. 3(e)]. Corrections estimated using gradients, which were found from the time series of differences between adjacent points, range within $\pm$10 cm/year, with a mean of 0.9 cm/year and a standard deviation of 1.7 cm/year.

Another important effect of the adjustment of the elevation time series is that it reduces the amplitude of seasonal elevation variation [4], [8]. Correcting elevation changes for their dependence on σ^0 reduced the seasonal peak-to-peak amplitude, on average, over the area of coverage from 27.5 $\pm$ 0.8 cm to 23.6 $\pm$ 0.6 cm, whereas accounting for all waveform shape parameters reduced the mean amplitude to 21.4 $\pm$ 0.6 cm. Thus, variations of all waveform shape parameters, in addition to changes of σ^0, contribute to the adjustment of the elevation time series on seasonal to decadal time scales.

The effects of the adjustment of the elevation time series for their dependence on σ^0 and other waveform shape parameters are illustrated using an example for an individual grid cell (see Fig. 4). Synchronous variations of dH and $d\sigma^0$ values are clearly seen over most of the time series [see Fig. 4(a)]. However, the rapid divergence of the time series in summer 2002 results in very low correlation coefficient and correlation gradient of 0.07 and 0.02 cm/dB, respectively. At the same time, the correlation coefficients before and after summer 2002 over the observed period are 0.84 and 0.76, and gradients are also significantly higher, amounting to 0.22 and 0.05 cm/dB. Thus, using the low gradient estimated from the whole time series will significantly underestimate the absolute values of corrections applied to every point of the elevation time series. The correlation and gradient estimated from the time series of the differences between adjacent points do not depend on the observed divergence between time series. Before and after summer 2002, they are very close to those obtained from the original time series (0.79 and 0.21 cm/dB before summer 2002 and 0.82 and 0.06 cm/dB after that) but remarkably higher for the whole time series, amounting to 0.11 cm/dB. The difference between gradients over the two periods indicates that the correlation gradient may significantly vary in time. These temporal variations and their influence on the adjustment of elevation time series will be considered in the next section.

Applying the improved estimate of the gradient allowed correcting the dH time series by better accounting for the relationship between elevation and σ^0 before and after summer 2002. However, the large elevation increase of several tens of centimeters in 2002 still remained and actually became even larger in the corrected time series due to the decrease of σ^0 at that time. As a result, the elevation change rate of 5.8 cm/year estimated from the adjusted elevation time series is 0.8 cm/year larger than that of the unadjusted time series. Such a correction is typical for the vast area in northeastern Greenland [see Fig. 3(d)] and is mainly caused by the σ^0 decrease in summer 2002 that is reflected in a negative σ^0 change rate [see Fig. 3(c)].

The considered cell is located in a low-accumulation area, and such a large elevation growth seems unrealistic especially during the summer of an increased melt anomaly. It is likely the result of the changes of the surface and subsurface scattering characteristics that influence the altimeter measurements. At the same time, the time series of two other waveform parameters, especially LeW, are more consistent during this period [see Fig. 4(a)]. The LeW decrease corresponds to the increased ratio between surface and subsurface backscattering that is typical in summer seasons when snow density is higher. The adjustment of the elevation time series for its dependence on all three waveform parameters substantially decreased the elevation increase during summer 2002 and reduced the elevation change rate to 3.4 cm/year. The seasonal peak-to-peak amplitude of the considered elevation time series is decreased from 31.3 cm for the unadjusted time series to 15.2 cm for the time series adjusted for correlation with σ^0 and to 9.5 cm for the time series adjusted for all waveform parameters.

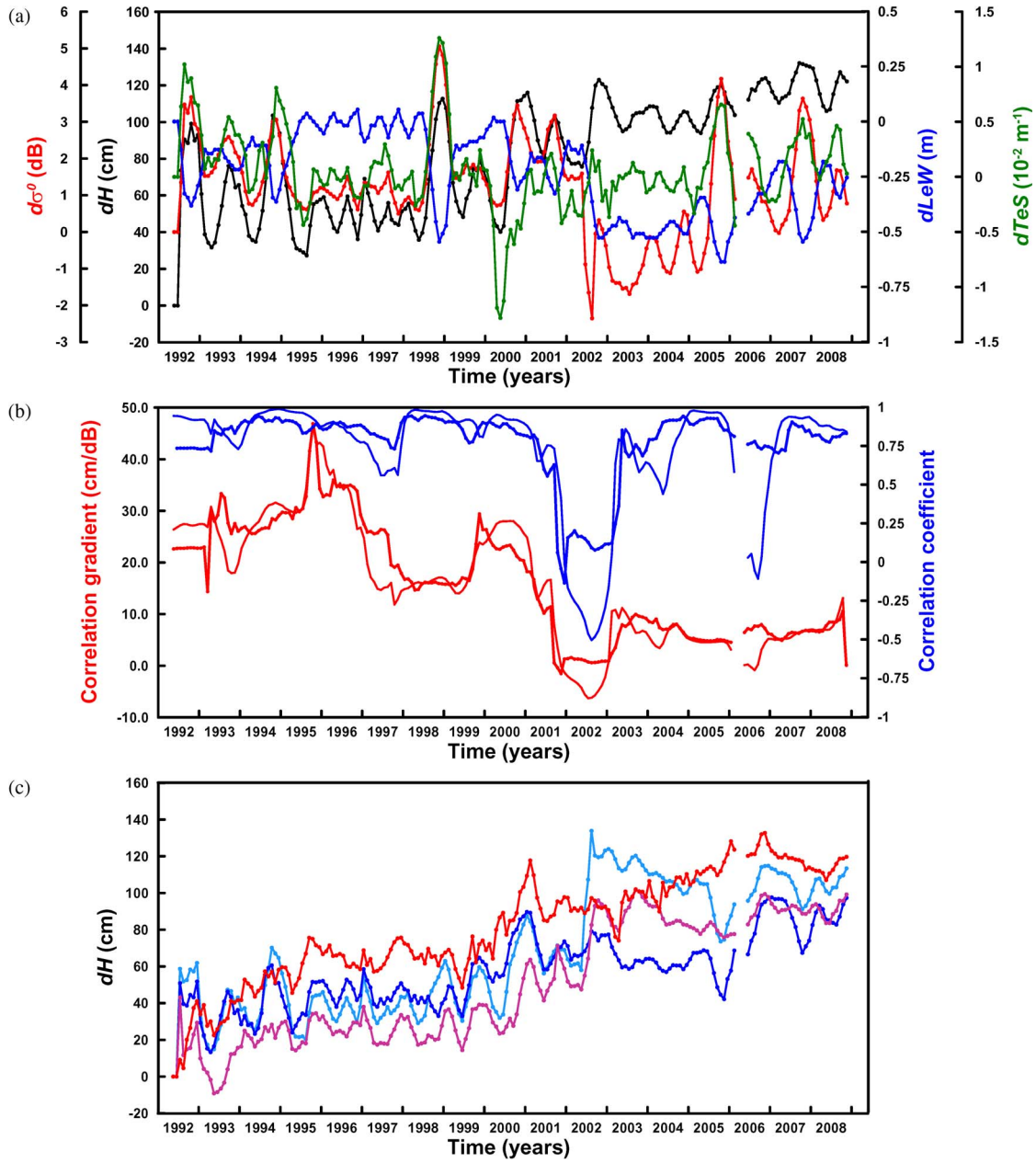

Fig. 4. Time series for the individual cell (79°–79.5° N and 34°–35° W) illustrating the adjustment of the elevation time series. (a) Unadjusted dH time series and three waveform parameters: σ^0, LeW, and TeS. (b) Time series of the correlation coefficient between elevation and σ^0 (blue) and corresponding correlation gradient (red) estimated for each point of the time series using surrounding consecutive points over 1.5-year time intervals from dH and $d\sigma^0$ values (thin lines) and ΔdH and $\Delta d\sigma^0$ values (thick lines). (c) dH time series adjusted for correlation with σ^0 using a constant gradient (light blue), with three waveform parameters using constant gradients (blue), with σ^0 using a temporally VCG (mauve), and with three waveform parameters using temporally VCGs (red).

B. Correction Using VCG

The method of adjustment of elevation time series for its dependence on backscatter power described previously implies using constant within-cell correlation gradients. However, the value of the gradient may vary not only spatially but also temporally because of the changes of the ice sheet surface properties in time. Although Davis and Ferguson [8] noted that they did not find a significant temporal variability of $dH/d\sigma^0$ over their five-year time series over the Antarctic ice sheet, this is clearly not the case when using 16.5-year time-series over the Greenland ice sheet. To estimate the temporal changes of the gradient, we calculated it for every point i of time series using several preceding and several following points: $\Delta dH_{i-k}, \ldots, \Delta dH_{i+k}$ and $\Delta d\sigma^0_{i-k}, \ldots, \Delta d\sigma^0_{i+k}$, where k is the number of ΔdH and $\Delta d\sigma^0$ points before and after point i.

Since the gradient may depend on both the interannual and seasonal variations, two estimations of the gradient were calculated. One estimation $(\Delta dH/\Delta d\sigma^0)_{\text{consecutive}}$ was obtained using consecutive points surrounding the point for which the gradient is calculated. In this case, $k = 8$ was used, i.e., the gradient for each point was calculated using 18 points (1.5 years) of time series. A 1.5-year interval was chosen because it corresponds to the highest correlation coefficient in average over the whole considered time period and over the whole of Greenland. The second estimation $(\Delta dH/\Delta d\sigma^0)_{\text{season}}$ was obtained from ΔdH and $\Delta d\sigma^0$ values related to the same

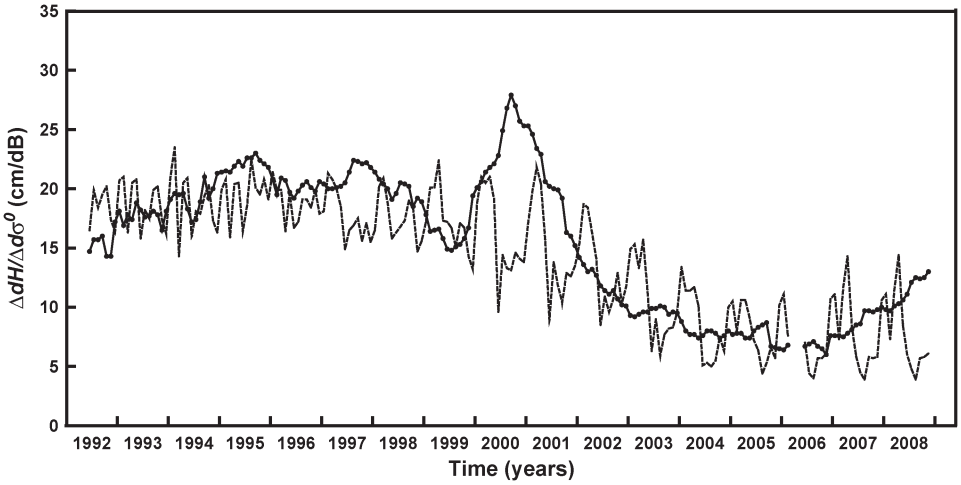

Fig. 5. Time series of the averaged (over the Greenland ice sheet) correlation gradients $\Delta dH/\Delta d\sigma^0$ estimated for each point of the time series using the surrounding consecutive points over 1.5-year time intervals $(\Delta dH/\Delta d\sigma^0)_{\mathrm{consecutive}}$ (solid line) and using the surrounding points related to the same months of every year over five-year time intervals $(\Delta dH/\Delta d\sigma^0)_{\mathrm{season}}$ (dotted line).

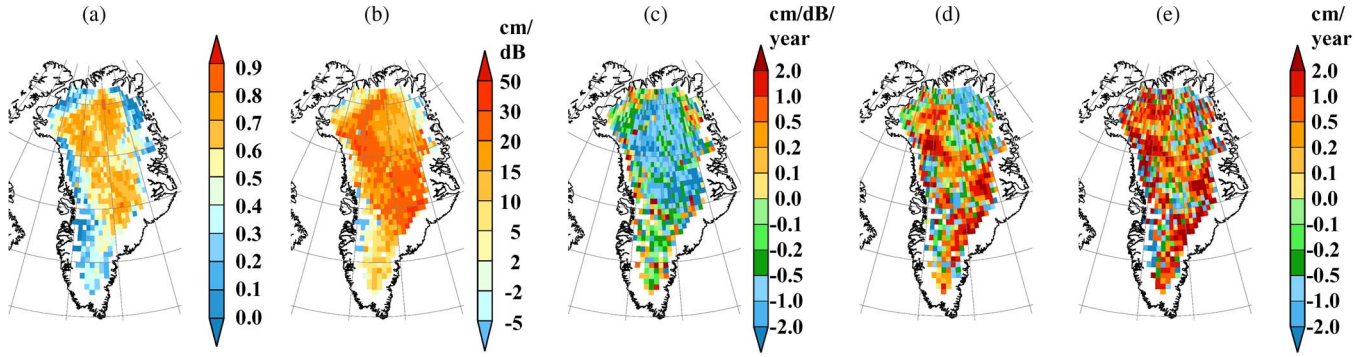

Fig. 6. Averaged within individual cells (a) correlation coefficients between ΔdH_i and $\Delta d\sigma_i^0$ values estimated for each point of the time series using 1.5-year time intervals, (b) corresponding correlation gradients, (c) change rates of these gradients, and corrections of dH/dt trends for changes in (d) σ^0 and (e) all waveform shape parameters calculated by applying temporally variable gradients.

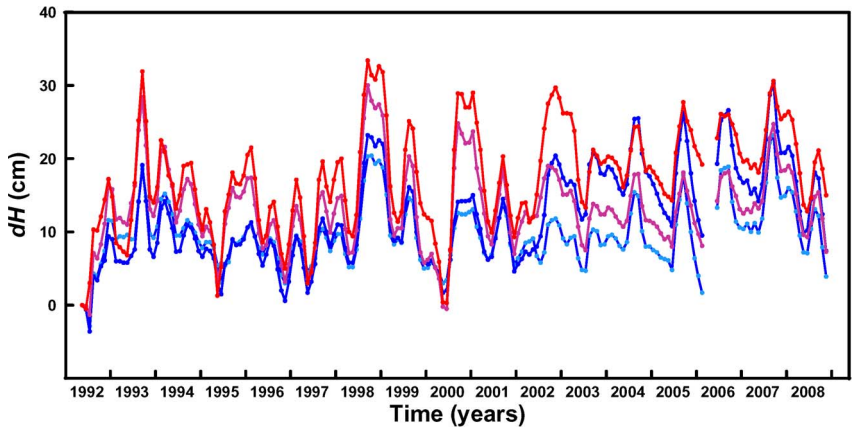

Fig. 7. Time series of the averaged (over the Greenland ice sheet) cumulated corrections of the elevation changes for the correlation with σ^0 obtained using a constant gradient (light blue), with all waveform parameters obtained using constant gradients (blue), with σ^0 obtained using a variable gradient (mauve), and with all waveform parameters obtained using variable gradients (red).

three-month interval (JFM or FMA or MAM, etc.) in different years in order to assess possible seasonality of the gradient. For the second estimation, $k = 2$ was used, i.e., five points (five years) for every three-month interval. If the number of available points required for the calculation of the gradient for any point was less than three for $(\Delta dH/\Delta d\sigma^0)_{\mathrm{season}}$ (observed in two cells) and five for $(\Delta dH/\Delta d\sigma^0)_{\mathrm{consecutive}}$ (observed in 16 cells for 1–10 points in each of the cell), then this gradient was assigned as zero to produce zero correction of elevation change for the corresponding point of time series.

The time series of the gradients averaged over Greenland show that gradient $(\Delta dH/\Delta d\sigma^0)_{\mathrm{consecutive}}$ better represents

interannual relative changes of ΔdH and $\Delta d\sigma^0$ but ignores any seasonal variations (see Fig. 5). The gradient $(\Delta dH/\Delta d\sigma^0)_{\text{season}}$ exhibits seasonal variations with typically higher values in winter and spring and lower values in summer and autumn, but it does not reveal rapid interannual fluctuations. Nevertheless, both gradients—$(\Delta dH/\Delta d\sigma^0)_{\text{consecutive}}$ and $(\Delta dH/\Delta d\sigma^0)_{\text{season}}$—indicate decadal changes with relatively high values before 2002, followed by the reduction of their values, where the minimum occurred in 2006. At the same time, Fig. 6(a) and (b) shows that the spatial distributions of the gradient $(\Delta dH/\Delta d\sigma^0)_{\text{consecutive}}$ and the corresponding correlation coefficients determined as averaged values for the whole time series over individual cells are generally in agreement. A similar agreement is observed for the gradient $(\Delta dH/\Delta d\sigma^0)_{\text{season}}$.

The indicated seasonal variations of the gradient $(\Delta dH/\Delta d\sigma^0)_{\text{season}}$ (see Fig. 5) confirm that the change of the ratio between the surface and the volume signal in the observed altimeter waveforms is the main reason for the correlation between the elevation and the backscattered power [6]. An increased snow densification and a larger size of the snow grains in the firn induced by a higher summer temperature result in smaller penetration of the part of the radar signal through the surface during summer and autumn, whereas during cold winters and springs, a larger signal penetration results in higher $(\Delta dH/\Delta d\sigma^0)_{\text{season}}$ values. The abrupt decrease of the gradient $(\Delta dH/\Delta d\sigma^0)_{\text{consecutive}}$ from 2002 (see Fig. 5) may represent the effect of lifting of the radar-reflection horizon proposed in [23] as a response to increased surface melting of the Greenland ice sheet in the 2000s. Although the effect of increased melting on elevation change during the last decade is indicated mostly over low-elevation margin areas, surface properties in the vast ice sheet interior areas may also be changed due to the observed increased melt extent [24], [25]. Thus, the time series of the correlation gradient likely reveal changes of the snowpack characteristics that are not reflected in backscattered power change.

Although the average time series of the gradient $(\Delta dH/\Delta d\sigma^0)_{\text{season}}$ helps in interpreting the observed changes of the correlation gradients, the small number of points (five points) in the time series distributed over a long time period (five years) does not allow estimating valuable gradients over individual cells. Therefore, the temporally variable correlation gradient (VCG) $(\Delta dH/\Delta d\sigma^0)_{\text{consecutive}}$ that was obtained from a larger amount of time series points and that better represents interannual gradient variations was used to adjust the elevation time series.

In order to take the temporal changes of the correlation gradient into account, a correction of elevation changes dH_i resulting from the correlation between elevation and σ^0 was determined over individual cells for each point i of time series as $(\Delta dH/\Delta d\sigma^0)_i \cdot d\sigma_i^0$, where $(\Delta dH/\Delta d\sigma^0)_i$ is the estimations of the VCG. Time series of $(\Delta dH/\Delta d\sigma^0)_i \cdot d\sigma_i^0$ values represent a cumulative correction, indicating its overall effect on the estimation of elevation change.

The average effect (over the coverage area) of adjusting the elevation time series for their correlation with σ^0 using VCG values on elevation change estimation is 0.14 cm/year, with a similar spatial distribution as that for the correction obtained using a constant gradient [see Fig. 6(d)]. At the same time, the time series of the averaged cumulated correction indicate remarkably larger seasonal variations than those obtained using a constant gradient over the period 1992–2002 and nearly the same for the period 2002–2008 (see Fig. 7), following the time series of the gradient (see Fig. 5). The VCG is larger than the constant gradient by ∼9 cm/dB before 2002 and smaller by only ∼2 cm/dB from 2002, decreasing with time over most of Greenland [see Fig. 6(c)] with an average rate of 0.88 cm/dB/year. The higher average VCG (15.3 ± 0.3 cm/dB) corresponding to a higher correlation coefficient (0.47 ± 0.01) is a result of considering short time intervals for the calculation of variable gradients and, therefore, a better agreement between the elevation and σ^0 time series. As a result, the average seasonal amplitude of the elevation time series adjusted for correlation with σ^0 using VCG is reduced to 20.1 ± 0.6 cm. Thus, the correction of elevation change determined as $(\Delta dH/\Delta d\sigma^0)_i \cdot d\sigma_i^0$ for each point of time series over individual cell is the result of superimposed gradient and σ^0 changes.

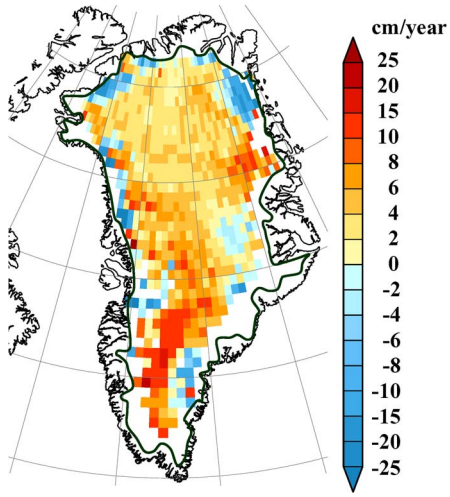

Fig. 8. Distribution of the dH/dt trends derived by merging ERS-1, ERS-2, and Envisat satellite altimeter measurements from 1992 to 2008 when applying temporally variable gradients to adjust the elevation time series for changes in waveform parameters. The line shows the boundaries of the ice sheet.

The sensitivity of the elevation change to the change in LeW and TeS also varies on different time scales. Applying the combined effect of σ^0, LeW and TeS changes on the elevation time series calculated for each point using the surrounding points over 1.5-year time span increases the correction, on average, up to 0.6 cm/year (see Figs. 6(e) and 7). The difference between the corrections is due mostly to the effect of the LeW change in summer 2002, and although it is not large, on average, it can locally be up to several centimeters per year. Thus, accounting for the variations of all waveform shape parameters in addition to changes of σ^0 contributed to the adjustment of the elevation time series. The combined effect of the elevation time series adjustment for their dependence on all waveform shape parameters and the use of VCG (i.e., temporally variable coefficients of multiple regression) decreases the seasonal amplitude to 16.0 ± 0.4 cm.

The effect of applying VCG for the adjustment of the elevation time series is shown for the example in Fig. 4. In contrast

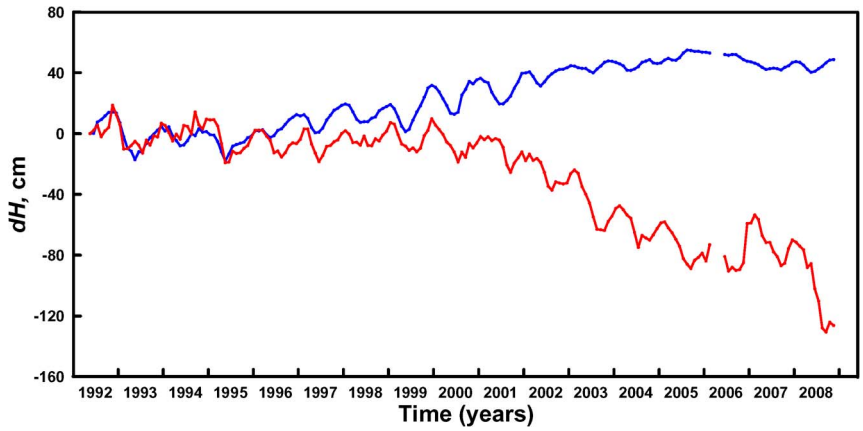

Fig. 9. Elevation time series over the areas above (blue) and below (red) 1500 m obtained by merging ERS-1, ERS-2 and Envisat satellite altimeter measurements from 1992 to 2008 when applying temporally variable gradients to adjust the elevation time series for changes of waveform parameters.

TABLE V
AVERAGE dH/dt TRENDS OVER DIFFERENT GREENLAND ICE SHEET AREAS DETERMINED BY APPLYING DIFFERENT CORRECTIONS FOR THE CHANGES OF THE WAVEFORM PARAMETERS

Region	Area, 10^3 km^2	Correction not applied	Correction applied			
			Constant gradients		Variable gradients	
			σ°	waveform	σ°	waveform
Whole Greenland	1328.1	3.4±0.2	3.2±0.2	2.5±0.2	3.3±0.2	2.8±0.2
> 1500 m	1182.1	4.7±0.2	4.4±0.2	3.7±0.2	4.5±0.2	4.0±0.2
< 1500 m	146.1	-6.9±0.9	-6.8±0.9	-7.1±0.9	-6.3±0.9	-7.0±1.0
West [a]	560.3	4.9±0.4	4.6±0.4	3.9±0.4	4.7±0.4	4.3±0.5
North-East [a]	632.5	2.4±0.3	2.4±0.2	1.7±0.2	2.5±0.2	1.9±0.3
South-East [a]	135.4	2.0±0.7	1.4±0.7	0.3±0.8	1.4±0.8	0.9±0.8

[a]Boundaries of the regions are outlined in Fig. 11

to constant gradients, variable gradients estimated from dH and $d\sigma^0$ values and from ΔdH and $\Delta d\sigma^0$ values for most of the time series do not differ significantly from each other [see Fig. 4(b)]. As was noted previously, the correlation gradient before 2002 is remarkably higher than that averaged over the considered time period and lower toward the end of the time series. While the low VCG values in 2002 are a result of a low correlation coefficient during this period, the high correlation coefficient over other years indicates that changes of the gradient represent changes of the sensitivity of the elevation time series to σ^0 variations. The influence of the gradient changes on the adjustment of the elevation time series is shown in Fig. 4(c). For example, applying high VCG values over the first five years of this period considered, when σ^0 decreases with a rate of 0.26 dB/year, resulted in a much faster elevation increase for the adjusted time series with a rate of 4.5 cm/year than the elevation change rate of 0.7 cm/year for the time series adjusted using a constant gradient.

The elevation increase in summer 2002 that was observed for the time series adjusted for the correlation with σ^0 using a constant gradient is smaller, but it is still present in the time series adjusted for the correlation with σ^0 using the VCG [see Fig. 4(c)]. The adjustment of the elevation time series for the dependence on all waveform parameters applying the VCG corrects this unrealistic elevation change, as was the case when using constant gradients. In addition, applying the VCG in adjusting the elevation time series for changes of all waveform parameters better represents their changes. For example, over the period 2003–2005, the time series adjusted using the VCG gives a substantially higher elevation change rate of 10.6 cm/year compared to the -3.5 cm/year obtained using constant gradients.

IV. ELEVATION CHANGE RESULTS

After the time series of the Greenland ice sheet surface elevation from 1992 to 2008 were formed, they were adjusted for the correlation between elevation and waveform parameters. The elevation time series, spatial distributions, and spatially averaged elevation change rates (dH/dt) obtained by applying corrections for correlation with waveform shape parameters estimated using VCG are shown in Figs. 8–11, and in Tables V and VI. An average elevation change rate of 2.8 cm/year was found over the area of coverage, which represents about 76% of the whole Greenland ice sheet, 87% of the area above 1500 m and only 38% of the margin areas below 1500 m, where the amount of available crossovers is limited (see Figs. 8 and 9, Table V). Therefore, involving

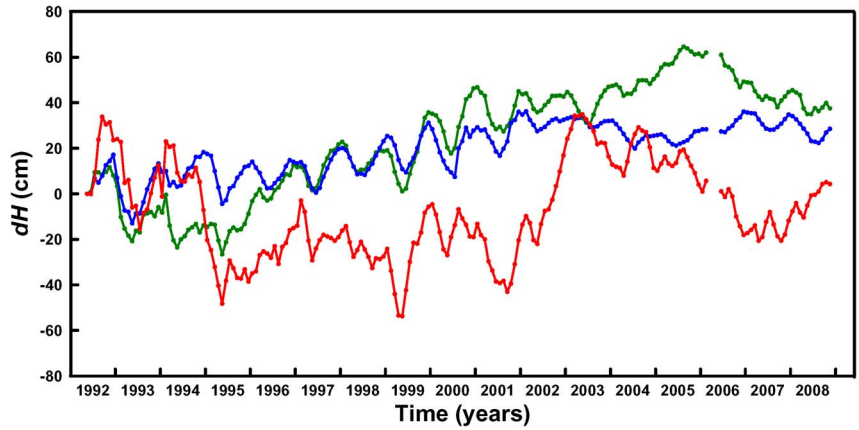

Fig. 10. Elevation time series obtained by merging ERS-1, ERS-2 and Envisat satellite altimeter measurements from 1992 to 2008 over western (green), northeastern (blue), and southeastern (red) zones of the Greenland ice sheet outlined in Fig. 11.

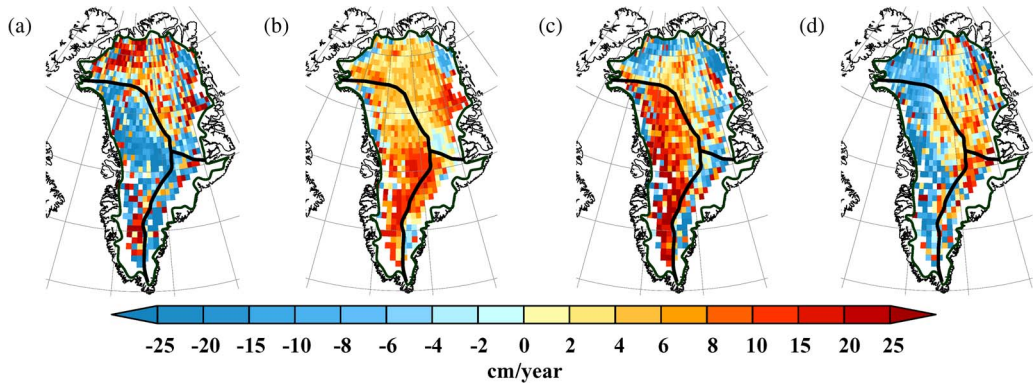

Fig. 11. Elevation change rates (dH/dt) (a) from AMJ 1992 to AMJ 1995, (b) from AMJ 1995 to AMJ 2003, (c) from JFM 2003 to JFM 2006, and (d) from OND 2005 to OND 2008. The ice divides (thick lines) and ice sheet boundaries (thin line) show the regions with different circulation regimes.

TABLE VI
AVERAGE dH/dt TRENDS OVER THREE GREENLAND ICE SHEET AREAS AND OVER DIFFERENT TIME PERIODS

	AMJ 1992 – AMJ 1995	AMJ 1995 – AMJ 2003	JFM 2003 – JFM 2006	OND 2005 – OND 2008
Whole Greenland	-3.9±0.8	5.1±0.3	2.0±0.6	-4.5±0.7
West [a]	-8.8±1.6	6.9±0.5	9.9±1.0	-9.2±1.4
North-East [a]	2.9±0.8	3.8±0.3	-3.1±0.6	-1.1±0.9
South-East [a]	-16.1±4.1	3.9±0.8	-7.1±2.3	-0.8±2.5

[a] is the same as in Table V

more coastal marginal areas would probably result in faster thinning over the areas below 1500 m than −7.0 cm/year for the whole considered period and −12.5 cm/year from OND 1999 to OND 2008. Increases in surface elevation that were observed over the central regions of Greenland from 1995 were followed by elevation decrease from 2006. In contrast, surface elevation decreases from 2000 in the low-elevation areas of the ice sheet have continued due to enhanced summer melting and are especially pronounced in 2008.

Although satellite radar altimetry does not allow investigating part of the ice sheet margin areas, combined ERS-1, ERS-2, and Envisat measurements provide a comparatively long elevation time series of the Greenland ice sheet with high spatial and temporal resolutions. Fig. 10 shows the elevation time series over three regions of Greenland that are generally governed by different regional circulation regimes. These regions are separated by the ice divides outlined in Fig. 11, which shows the spatial distributions of the dH/dt results over different time periods. Western and southeastern parts of Greenland, where accumulation is influenced by the Icelandic Low and the Baffin Bay Low, exhibit the most significant interannual elevation variations. Over the low-accumulation northeastern area, mostly seasonal variations are indicated. The largest elevation variability is indicated in the southeastern area, where the largest precipitations and high ice sheet flow velocities are observed. The elevation time series indicate a strong elevation decrease before 1995 for the west and southeast areas but show remarkable differences for the period from 1995 (see Figs. 10 and 11 and Table VI). Among the elevation variations over the southeastern area it can be noted

a sharp elevation increase in 2002–2003 that is consistent with the airborne laser altimeter measurements [26] and apparently caused by enhanced accumulation [27]. Another feature of the time series in this area is an elevation decrease from 2005 to the end of 2006, which is in qualitative agreement with the results from model studies of accumulation [28]. Moderate ice sheet growth over the western area from 1995 to 2003 changed to a rapid elevation increase that lasted until 2006 and was followed by a rapid elevation decrease. These changes on the west side of Greenland can also be explained by relatively high and low (modeled) accumulations over Greenland in 2005 and 2006, respectively [28].

V. Conclusion

The Greenland ice sheet elevation changes for a 16.5-year time period from 1992 to 2008 have been analyzed here from the ERS-1, ERS-2, and Envisat satellite radar altimeter data. Continuous elevation and waveform parameter time series were created by applying intersatellite biases to crossover differences. Because biases are not spatially invariant over Greenland, the method that utilizes an amount of data that is sufficient to allow calculating biases over individual grid cells (1° longitude $\times$ 0.5° latitude) was developed. A significant effect of AD bias on intersatellite biases was revealed and taken into account when creating the time series. The largest and smallest ERS-1/ERS-2 and ERS-2/Envisat elevation biases are observed over margins and in the central areas, respectively, and vary over the Greenland ice sheet from -1.8 to 3.4 m. Corresponding σ^0 biases are negative everywhere and range from -9.8 to -1 dB. The ERS-2/Envisat biases of waveform parameters LeW and TeS also vary significantly, ranging from -3.8 to 0.2 m and from -0.14 to 0.02 m^{-1}, respectively.

Creating time series of waveform parameters was performed in order to account for variations in the ice sheet surface properties by adjusting the elevation time series for changes of waveform parameters. Although the adjustment of the elevation changes depends primarily on the variations of σ^0, other waveform shape parameters also contributed to the correction for changes in surface and subsurface scattering characteristics. It was found that the correction depends not only on the temporal variations of the waveform parameters but also on the temporal variations of the correlation gradients, which represent the sensitivity of the elevation change to the change in waveform parameters. For σ^0, on average, over the Greenland ice sheet, relatively high and low gradients are observed, respectively, before and after 2002. In addition, as gradients were calculated for parts of the time series, they are, on average, higher than the gradients determined from the whole time series, resulting in higher absolute corrections applied to every point of the time series. Both—the adjustment of the elevation time series for the combined effect of waveform parameters' variations in addition to accounting for only σ^0 changes as well as using temporally variable gradients—resulted in a decrease in the seasonal amplitude of elevation time series. The average seasonal peak-to-peak amplitude of the adjusted elevation time series over the area of coverage is of 16.0 cm, whereas the unadjusted time series have an average amplitude of 27.5 cm.

An elevation change rate (dH/dt) of 2.8 cm/year in the interior of Greenland covering 76% of the ice sheet area from 1992 to 2008 was found. Increases in surface elevation that were observed over the high-elevation regions from 1995 were followed by an elevation decrease from 2006. In contrast, surface elevation decreases from 2000 in the low-elevation areas of the ice sheet have continued due to enhanced summer melting and are especially pronounced in 2008. Over 87% of the high-elevation areas above 1500 m, an elevation increase is 4.0 ± 0.2 cm/year. An elevation decrease with a rate of -7.0 ± 1.0 cm/year represents only 38% of the areas below 1500 m, and involving more coastal areas would result in faster thinning than about -12 cm/year indicated from 2000. Because marginal areas are not completely measured by radar altimetry, substantial thinning rates over these areas could offset the elevation change observed in this paper. At the same time, longer elevation time series are required to establish long-term trends as large interannual elevation variability is observed.

Acknowledgment

The author would like to thank NASA/GSFC for providing the altimeter data used in this paper, F. Remy and B. Legresy for the useful discussions of the results, the two anonymous referees for their numerous comments that greatly improve this paper, and M. Miles for improving the language.

References

[1] R. B. Alley, M. K. Spencer, and S. Anandakrishnan, "Ice-sheet mass balance: Assessment, attribution and prognosis," *Ann. Glaciol.*, vol. 46, no. 1, pp. 1–7, Oct. 2007.

[2] K. S. Khvorostovsky, L. P. Bobylev, and O. M. Johannessen, "Greenland ice sheet elevation variations," in *Arctic Environment Variability in the Context of Global Change*, L. P. Bobylev, K. Y. Kondratyev, and O. M. Johannessen, Eds. Chichester, U.K.: Springer-Praxis, 2003, pp. 270–281.

[3] O. M. Johannessen, K. Khvorostovsky, M. W. Miles, and L. P. Bobylev, "Recent ice-sheet growth in the interior of Greenland," *Science*, vol. 310, no. 5750, pp. 1013–1016, Nov. 2005.

[4] H. J. Zwally, M. B. Giovinetto, J. Li, H. G. Cornejo, M. A. Beckley, A. C. Brenner, J. L. Saba, and D. Yi, "Mass changes of the Greenland and Antarctic ice sheets and shelves and contributions to sea-level rise: 1992–2002," *J. Glaciol.*, vol. 51, no. 175, pp. 509–527, 2005.

[5] Y. Li and C. H. Davis, "Decadal mass balance of the Greenland and Antarctic ice sheets from high resolution elevation change analysis of ERS-2 and Envisat radar altimetry measurements," in *Proc. 28th Geosci. Remote Sens. Symp.*, Boston, MA, 2008, pp. IV-339–IV342.

[6] B. Legrésy and F. Rémy, "Using the temporal variability of satellite radar altimetric observations to map surface properties of the Antarctic ice sheet," *J. Glaciol.*, vol. 44, no. 147, pp. 197–206, 1998.

[7] D. J. Wingham, A. L. Ridout, R. Scharroo, R. J. Arthern, and C. K. Shum, "Antarctic elevation change from 1992 to 1996," *Science*, vol. 282, no. 5388, pp. 456–458, Oct. 1998.

[8] C. H. Davis and A. C. Ferguson, "Elevation change of the Antarctic ice sheet, 1995-2000, from ERS-2 satellite radar altimetry," *IEEE Trans. Geosci. Remote Sens.*, vol. 42, no. 11, pp. 2437–2445, Nov. 2004.

[9] P. Lacroix, B. Legrésy, F. Rémy, F. Blarel, G. Picard, and L. Brucker, "Rapid change of snow surface properties at Vostok, East Antarctica, revealed by altimetry and radiometry," *Remote Sens. Environ.*, vol. 133, no. 12, pp. 2633–2641, 2009.

[10] A. C. Brenner, H. J. Zwally, H. G. Cornejo, and J. L. Saba, "Investigation of correlations between variations of radar backscatter with altimeter-derived ice sheet elevation changes and ERS-2/ERS-1 biases," in *Proc. ESA ERS-Envisat Symp.*, Gothenburg, Sweden, 2000.

[11] B. Legrésy, F. Rémy, and P. Schaeffer, "Different ERS altimeter measurements between ascending and descending tracks caused by wind induced features over ice sheets," *Geophys. Res. Lett.*, vol. 26, pp. 2231–2234, 1999.

[12] R. J. Arthern, D. J. Wingham, and A. L. Ridout, "Controls on ERS altimeter measurements over ice sheets: Footprint-scale topography, backscatter fluctuations, and the dependence of microwave penetration depth on satellite orientation," *J. Geophys. Res.*, vol. 106, no. D24, pp. 33 471–33 484, 2001.

[13] F. Rémy, B. Legrésy, and J. Benveniste, "On the azimuthally anisotropy effects of polarization for altimetric measurements," *IEEE Trans. Geosci. Remote Sensing*, vol. 44, no. 11, pp. 3289–3296, Nov. 2006.

[14] C. H. Davis, Y. Li, J. R. McConnell, M. M. Frey, and E. Hanna, "Snowfall-driven growth in East Antarctic ice sheet mitigates recent sea-level rise," *Science*, vol. 308, no. 5730, pp. 1898–1901, May 2005.

[15] B. Legrésy and F. Rémy, "Surface characteristics of the Antarctic ice sheet and altimetric observations," *J. Glaciol.*, vol. 43, no. 144, pp. 265–275, 1997.

[16] H. J. Zwally and A. C. Brenner, "Ice sheet dynamics and mass balance," in *Satellite Altimetry and Earth Sciences: A Handbook of Techniques and Applications*. Orlando, FL: Academic, 2001, ch. 9, pp. 351–369.

[17] A. C. Brenner, J. P. DiMarzio, and H. J. Zwally, "Precision and accuracy of satellite radar and laser altimeter data over the continental ice sheets," *IEEE Trans. Geosci. Remote Sens.*, vol. 45, no. 2, pp. 321–331, Feb. 2007.

[18] K. Khvorostovsky and O. M. Johannessen, Merging of ERS-1, ERS-2 and Envisat altimeter data over the Greenland ice sheet, Nansen Environ. Remote Sens. Center, Bergen, Norway, Tech. Rep. 307. [Online]. Available: http://www.nersc.no/sites/www.nersc.no/files/Report307.pdf

[19] Eur. Space Agency/Eur. Space Res. Inst., Tech. Note ER-TN-RS-RA-0022 P. Femenias, ERS QLOPR and OPR range processing, Frascati, Italy1997, Tech. Note ER-TN-RS-RA-0022.

[20] C. K. Shum, Y. Yuchan, A. Braun, K. Cheng, and S. Calmant, "Over ocean Cal/Val of Envisat radar altimeter and geophysical data record algorithms," European Space Agency, Paris, France, Final Rep., 2003.

[21] Y. Li and C. H. Davis, "Improved methods for analysis of decadal elevation-change time series over Antarctica," *IEEE Trans. Geosci. Remote Sens.*, vol. 44, no. 10, pp. 2687–2697, Oct. 2006.

[22] D. J. Wingham, A. Shepherd, A. Muir, and G. J. Marshall, "Mass balance of the Antarctic ice sheet," *Philos. Trans. R. Soc. A*, vol. 364, no. 1844, pp. 1627–1635, Jul. 2006.

[23] R. H. Thomas, C. H. Davis, E. Frederick, W. Krabill, Y. Li, S. Manizade, and C. Martin, "A comparison of Greenland ice sheet volume changes derived from altimetry measurements," *J. Glaciol.*, vol. 54, no. 185, pp. 203–212, Mar. 2008.

[24] K. Steffen, S. V. Nghiem, R. Huff, and G. Neumann, "The melt anomaly of 2002 on the Greenland ice sheet from active and passive microwave satellite observations," *Geophys. Res. Lett.*, vol. 31, p. L20 402, Oct. 2004, DOI:10.1029/2004GL020444.

[25] M. Tedesco, "Snowmelt detection over the Greenland ice sheet from SSM/I brightness temperature daily variations," *Geophys. Res. Lett.*, vol. 34, p. L02 504, Jan. 2007, DOI:10.1029/2006GL028466.

[26] W. Krabill, E. Hanna, P. Huybrechts, W. Abdalati, J. Cappelen, B. Csatho, E. Frederick, S. Manizade, C. Martin, J. Sonntag, R. Swift, R. Thomas, and J. Yungel, "Greenland ice sheet: Increased coastal thinning," *Geophys. Res. Lett.*, vol. 31, p. L24 402, Dec. 2004, DOI:10.1029/2004GL021533.

[27] E. Hanna, J. McConnell, S. Das, J. Cappelen, and A. Stephens, "Observed and modeled Greenland ice sheet snow accumulation, 1958–2003, and links with regional climate forcing," *J. Climate*, vol. 19, no. 3, pp. 344–358, Feb. 2006.

[28] E. W. Burgess, R. R. Forster, J. E. Box, E. Mosley-Thompson, D. H. Bromwich, R. C. Bales, and L. C. Smith, "A spatially calibrated model of annual accumulation rate on the Greenland Ice Sheet (1958-2007)," *J. Geophys. Res.*, vol. 115, no. F2, p. F02 004, Apr. 2010. DOI:10.1029/2009JF001293.

Kirill S. Khvorostovsky received the Ph.D. degree in climatology and meteorology from St. Petersburg State University, St. Petersburg, Russia, in 2005.

Since 2006, he has been with the Nansen Environmental and Remote Sensing Center, Bergen, Norway. His research interests are in the area of remote sensing of the Greenland ice sheet.